GPS Solutions (2018) 22:94
https://doi.org/10.1007/s10291-018-0758-2

ORIGINAL ARTICLE

Ionospheric deformation of broadband GNSS signals and its analysis with a high gain antenna

Ulrich Hörmann[1] · Steffen Thoelert[1,2] · Matteo Sgammini[1] · Christoph Enneking[1] · Johann Furthner[1] · Michael Meurer[1,2] · Felix Antreich[1,3]

Received: 7 February 2017 / Accepted: 2 July 2018 / Published online: 10 July 2018

Abstract
The ionospheric delay of global navigation satellite systems (GNSS) signals typically is compensated by adding a correction value to the pseudorange measurement. We examine the ionospheric signal distortion beyond a constant delay. These effects become increasingly significant with increasing signal bandwidth and hence more critical for the new broadband navigation signals. By simulation, we first demonstrate that the signal modulation constellation diagram is particularly susceptible to the influence of the ionosphere already at moderate electron content. Using high gain antenna measurements of the Galileo E5 signal, we then verify that the expected influence can indeed be observed and compensated. A new method based on a binned maximum likelihood estimator is derived to estimate the total electron content (TEC) from a single frequency high gain antenna measurement of a broadband GNSS signal. Results of the estimation process are presented and discussed comparing to common TEC products such as TEC maps and dual-frequency receiver estimates.

Keywords GNSS · Navigation signals · Galileo E5 · Ionosphere estimation · TEC · Total electron content estimation · Remote sensing · Ionospheric signal deformation

Introduction

Satellite navigation applications range from mobile user positioning up to safety critical application in transportation systems such as airplanes, ships or future advanced driving assistance systems. Therefore, it is necessary to ensure the high quality of the service, and consequently, the transmitted satellite signals have to be observed and analyzed constantly. The basis for any analysis is global navigation satellite systems (GNSS) signal measurements captured by receiving systems using low gain omnidirectional or high gain antenna systems. For the data analysis to assess the transmitted signal quality, it is essential to compensate for the behavior of the measurement system (system calibration).

✉ Steffen Thoelert
steffen.thoelert@dlr.de

[1] Institute of Communications and Navigation, German Aerospace Center (DLR), Oberpfaffenhofen, Germany

[2] Chair of Navigation, RWTH Aachen University, Aachen, Germany

[3] Department of Teleinformatics Engineering, Federal University of Ceará (UFC), Fortaleza, Brazil

Additionally, either for the ordinary user or in case of signal quality analysis, it is necessary to eliminate signal propagation effects resulting from the signal traveling through the atmosphere. One of the important impacts on the ray path is caused by the ionosphere. The commonly determined ionospheric property is the total electron content (TEC). This value can be derived using various methods, e.g., probes, interferometric techniques, or GNSS dual-frequency measurement analysis. Ionospheric TEC measurements using GNSS observables have been performed for more than 20 years (Sardòn et al. 1994, Jakowski 1996; Hernandéz-Pajares et al. 1999).

In addition to the mentioned methods of TEC estimation, broadband in-phase and quadrature (I–Q) sample data taken by a high gain antenna system can also be used to determine the ionospheric TEC. The motivation for our work is based on the need for TEC compensation for satellite in-orbit tests at the beginning of the life of a space vehicle. In the early life of the space vehicle, the range biases based on satellite hardware effects, are not known yet, and thus cannot be compensated in real-time dual-frequency measurements. Thus, only TEC products such as TEC maps could be used to compensate for ionospheric dispersion. However, within the

conversion from the so-called slant TEC (sTEC) to the vertical TEC (vTEC; measure in TEC maps) during processing of the maps as well as from vTEC into sTEC, which is finally used for the data calibration, uncertainties get into the TEC estimates. These errors that are caused by the mapping from vTEC to sTEC or vice versa are considered to be too high for the application at hand. Therefore, in this application, TEC maps are not commonly used for ionospheric compensation of measurement data.

Instead, high gain antenna data are used to estimate the ionospheric dispersion directly and to compensate the influence of the ionosphere on the signal. We propose a maximum likelihood estimator for TEC and received power based on binned data to correct ionospheric effects in signal quality monitoring for in-orbit validation. We compare the results of the proposed estimator to TEC maps and dual-frequency measurements performed simultaneously with a GNSS receiver connected to the high gain antenna. We perform appropriate satellite bias estimation for the considered satellite and GNSS receiver to compensate for this bias in the dual-frequency measurements. Furthermore, the proposed method and its results can be used to verify TEC measurements based on other methods (probes, GNSS dual frequency). Especially for lower elevations of less than 20°, it could be helpful as a crosscheck for TEC maps conversion methods.

Theory

While the ionospheric delay is a well-known issue in the global navigation satellite systems (GNSS) community, this term has to be regarded as an oversimplification of the underlying physical effects. It is, therefore, instructive to recapitulate these effects in detail before we turn towards their implications from a signal processing perspective:

The ionosphere is a part of the earth's atmosphere which starts at about 50 km and extends roughly to a height of 1000 km (Zolesi and Cander 2014). In this part of the atmosphere, solar radiation ionizes a fraction of the present molecules and hence generates a plasma (Kelley 2009). For radio signals traveling from space to earth or vice versa this conductive layer represents a dispersive medium whose dispersion relation is in first approximation, i.e., neglecting the influence of the earth magnetic field, given by Garbuny (1965):

$$\omega^2 = k^2c^2 + \omega_\mathrm{p}^2 \tag{1}$$

Here, ω is the angular frequency of the electromagnetic wave, k is the wavenumber, c is the speed of light in vacuum and ω_p is the angular plasma frequency.

Common ionosphere considerations, especially in the field of precise positioning, also contain second and third order approximations of the ionospheric effects. Both terms are related to the electron content along the signal propagation path. Moreover, the second and third order terms are associated with the influence of the geomagnetic field on the ionospheric refractive index, the TEC value and the spatial distribution of the local electron density along the signal path. In addition, there are ray bending effects in consideration of the ionospheric impact on different frequencies. Hoque and Jakowski (2008) shows that ray bending effects are within millimeter range for GPS L1 and L2. This leads us to assume that these effects are negligible in the present work due to the relatively small frequency difference within one single frequency band compared to different frequency bands. In highly active ionospheric regions such as the equatorial regions, the sum of the higher order terms can result in several centimeter signal delay or a few TEC units (TECU) (Marques et al. 2012). Our station is located at middle latitudes in central Europe. In this region, the ionospheric activity is usually low in no-ionospheric storm conditions. The resulting TEC based on second and third order calculations should be significantly below 1 TECU (Hoque and Jakowski 2008) and, therefore, can be assumed negligible.

The angular plasma frequency ω_p depends on the electron density n_e and is given by:

$$\omega_\mathrm{p} = 2\pi f_\mathrm{p} = \sqrt{\frac{n_\mathrm{e}e^2}{\varepsilon_0 m_\mathrm{e}}} \tag{2}$$

where e is the elementary charge, ε_0 the vacuum permittivity and m_e denotes the electron mass. Using the respective definition, $v_\mathrm{p} = \omega/k$ and $v_\mathrm{g} = \partial\omega/\partial k$, the phase and group velocity can be calculated from (1) as:

$$v_\mathrm{p} = \frac{c}{\sqrt{1 - f_\mathrm{p}^2/f^2}} \approx c\left(1 + \frac{1}{2}\frac{f_\mathrm{p}^2}{f^2}\right) > c \tag{3}$$

$$v_\mathrm{g} = c\sqrt{1 - f_\mathrm{p}^2/f^2} \approx c\left(1 - \frac{1}{2}\frac{f_\mathrm{p}^2}{f^2}\right) < c \tag{4}$$

The corresponding phase and group refractive indices $n = c/v$ can be derived, accordingly:

$$n_\mathrm{p} = \sqrt{1 - f_\mathrm{p}^2/f^2} \approx \left(1 - \frac{1}{2}\frac{f_\mathrm{p}^2}{f^2}\right) \tag{5}$$

$$n_\mathrm{g} = \frac{1}{\sqrt{1 - f_\mathrm{p}^2/f^2}} \approx \left(1 + \frac{1}{2}\frac{f_\mathrm{p}^2}{f^2}\right) \tag{6}$$

As a central result, these quantities are dependent on the frequency f manifesting that the ionosphere is a dispersive medium indeed. It is worth noting that phase velocity and group velocity of the traveling signal are in opposite direction. In particular, the phase velocity becomes faster than the speed of light in vacuum, while the group velocity is reduced by the medium. This is the cause of what is generally known as phase advance and group delay: if the transit time T of a signal from a sender S to a receiver R is measured, then its carrier (traveling at v_p) will arrive earlier (advance), while the modulated information (traveling at v_g) will arrive later (delay) compared to the same signal traveling in vacuum. For distance measurements, where a constant propagation velocity equal to the speed of light in vacuum c is assumed, this wave dispersion results in an apparent range that differs from the Euclidean distance X and is denoted as the optical path length X_opt. Physically, this is a direct consequence of Fermat's principle of least time which can be used to calculate the optical path length from the corresponding refractive index:

$$T = \int_{t_\mathrm{S}}^{t_\mathrm{R}} \mathrm{d}t = \frac{1}{c}\int_{t_\mathrm{S}}^{t_\mathrm{R}} \frac{c}{v}\frac{\mathrm{d}x}{\mathrm{d}t}\,\mathrm{d}t = \frac{1}{c}\int_{x(t_\mathrm{S})}^{x(t_\mathrm{R})} n\,\mathrm{d}x \tag{7}$$

Hence, the optical path length is given by the integral of the refractive index n along the propagation path:

$$X_\mathrm{opt} = cT = \int_{x_\mathrm{S}}^{x_\mathrm{R}} n\,\mathrm{d}x \tag{8}$$

Note in particular that the optical path length equals the Euclidean distance if $n = 1$, i.e. in vacuum. The phase advance as well as group delay can thus be expressed as the difference ΔX between the optical path length and the Euclidean distance:

$$\Delta X = X_\mathrm{opt} - X = \int_{x_\mathrm{S}}^{x_\mathrm{R}} (n-1)\,\mathrm{d}x \tag{9}$$

Combining (5) and (9) the phase advance can be calculated as:

$$\begin{aligned}\Delta X_\mathrm{p} &= \int_{x_\mathrm{S}}^{x_\mathrm{R}} (n_\mathrm{p}-1)\,\mathrm{d}x \approx \int_{x_\mathrm{S}}^{x_\mathrm{R}} -\frac{1}{2}\frac{f_\mathrm{p}^2}{f^2}\,\mathrm{d}x \\ &= -\frac{e^2}{8\pi^2\epsilon_0 m_\mathrm{e}}\frac{1}{f^2}\int_{x_\mathrm{S}}^{x_\mathrm{R}} n_e\,\mathrm{d}x = -\frac{e^2}{8\pi^2\epsilon_0 m_\mathrm{e}}\frac{1}{f^2}\ \mathrm{TEC}\end{aligned} \tag{10}$$

The path integral of the electron density is denoted as the total electron content (TEC) and is of dimension $1/\mathrm{m}^2$. Quite analogously to (10) an expression for the group delay can be derived. If the constant factor is evaluated numerically, then the phase advance and group delay read:

$$\Delta X_\mathrm{p} = -40.3\,\frac{m^3}{s^2}\frac{\mathrm{TEC}}{f^2} \tag{11}$$

$$\Delta X_\mathrm{g} = +40.3\,\frac{m^3}{s^2}\frac{\mathrm{TEC}}{f^2} \tag{12}$$

In agreement with what was derived from the phase and group velocity, phase advance and group delay are equal in size but opposite in direction.

It is important to note that the total electron content as defined in (10) is specific to the relative geometry between the transmitter and receiver, and cannot be regarded as an intrinsic property of the ionosphere. This quantity is, therefore, sometimes denoted as sTEC and can be measured by dual-frequency GNSS receivers (Jakowski et al. 2011). Within the framework of a thin-shell model, the sTEC can then be used to calculate the equivalent vTEC as an ionospheric property at the geographic location of the so-called ionospheric pierce point (Ya'acob et al. 2008). Since the electron density builds up during the day but decreases at night, when recombination of charged particles outweighs the generation, the TEC is typically dependent on the time of day, the time of year and on the geographic latitude as well as the solar flux (Zolesi and Cander 2014). Single frequency receivers, therefore, have to rely on externally generated, up-to-date vTEC maps or empirical ionosphere models to correct for the ranging errors introduced by the ionosphere (Klobuchar 1987, European GNSS OS 2015).

In a GNSS receiver the corrections for the phase advance and the group delay are usually corrected by a single value added or subtracted to the code phase and carrier phase pseudorange measurement. However, this neglects the dispersive nature of the ionosphere, especially for broadband signals. In this work, we explore how the dispersive nature of the ionosphere is affecting broadband signals, in particular, how the so-called signal constellation diagram is affected. We assess these effects based on simulations and based on high-gain antenna measurements. Furthermore, we will present a new method to estimate sTEC based on single frequency high-gain antenna measurements, and we show that based on these estimates the dispersive nature of the ionosphere can be taken into account for ionospheric corrections of broadband GNSS signals. Such an analysis, the estimation of sTEC, and the ionospheric corrections for broadband signals are especially interesting for signal quality monitoring (SQM) and signal verification using high-gain antennas.

Below we define the signal model after propagating through the ionosphere and after down conversion to baseband. Afterwards, we will derive an estimator for single frequency sTEC estimation based on binned-data (signal constellation diagram). Finally, we will assess the dispersive effect of the ionosphere in broadband signals, and we will analyze the performance of our new approach to estimate sTEC based on high-gain antenna measurements.

Signal model

A digitally modulated pass band GNSS signal transmitted by a satellite can be given by:

$$\tilde{y}(t) = \sqrt{P_\mathrm{t}}\left(y_\mathrm{I}(t)\cos\left(2\pi f_\mathrm{c} t\right) - y_\mathrm{Q}(t)\sin\left(2\pi f_\mathrm{c} t\right)\right) \tag{13}$$

where $y_\mathrm{I}(t)$ is the so-called inphase component and $y_\mathrm{Q}(t)$ is the quadrature component. P_t is the transmit power and f_c is the carrier frequency of the signal. The Fourier transform of $\tilde{y}(t)$ is denoted by $\mathcal{F}\{\tilde{y}(t)\} = \tilde{Y}(f)$, moreover, the respective inverse Fourier transform is given by $\mathcal{F}^{-1}\left\{\tilde{Y}(f)\right\} = \tilde{y}(t)$. Propagation of the signal through the ionosphere can be approximated following (12) by the transfer function:

$$H(f;\mathrm{TEC}) = e^{j2\pi f \Delta T(f;\mathrm{TEC})} \tag{14}$$

with $\Delta T(f;\mathrm{TEC}) = \Delta X_\mathrm{g}/c$. Please note, that the inverse Fourier transform of $H(f;\,\mathrm{TEC})$ cannot be derived since the integral $\int_{-\infty}^{\infty} H(f;\mathrm{TEC})\mathrm{e}^{j2\pi ft}\mathrm{d}f$ does not converge. However, the inverse Fourier transform of $\tilde{Y}(f)H(f;\mathrm{TEC})$ can be derived in case $\tilde{y}(t)$ is bandlimited to the single-sided bandwidth B and $f_\mathrm{c} > B$. In the following, besides the ionosphere, we only consider free space path-loss L, and no other effects caused by the troposphere, multipath, etc. Following Hobinger and Jakowski (2017) the troposphere can be considered to be a nondispersive medium in L-band and consequently the troposphere delay effects are identical for group and phase delay observations. Thus, the troposphere does not affect estimates of the sTEC based on the dispersion influencing GNSS signals. Multipath can be neglected, since the beamwidth of the high-gain antenna pattern is very small and the sidelobe to mainlobe gain ratio is large.

Thus, the received signal after propagating from the satellite to the receiver on earth can be given by:

$$\sqrt{LG_\mathrm{r}G_\mathrm{t}}\,\tilde{Y}(f)H(f;\mathrm{TEC}) = \frac{\sqrt{P_\mathrm{r}}}{2}Y\left(f-f_\mathrm{c}\right)H(f;\mathrm{TEC}) + \frac{\sqrt{P_\mathrm{r}}}{2}Y^*\left(f+f_\mathrm{c}\right)H(f;\mathrm{TEC}) \tag{15}$$

where G_r is the gain of the receive antenna, G_t is the gain of the transmit antenna, $P_\mathrm{r} = P_\mathrm{t}L\,G_\mathrm{r}G_\mathrm{t}$ is the received power, $Y(f) = Y_\mathrm{I}(f) + jY_\mathrm{Q}(f)$, $\mathcal{F}\left\{y_\mathrm{I}(t)\right\} = Y_\mathrm{I}(f)$, and $\mathcal{F}\left\{y_\mathrm{Q}(t)\right\} = Y_\mathrm{Q}(f)$. Performing down conversion of the signal by multiplying the passband signal with either $2\cos(2\pi f_\mathrm{c}t)$ or $-2\sin\left(2\pi f_\mathrm{c}t\right)$ and the subsequent low-pass filtering with

$$\mathcal{F}\{h_\mathrm{L}(t)\} = H_\mathrm{L}(f) = \begin{cases} 1, & |f| \le B \\ 0, & |f| > B \end{cases} \tag{16}$$

as depicted in Fig. 1, we get:

$$\mathcal{F}\{s_\mathrm{I}(t;\boldsymbol{\theta})\} = \frac{\sqrt{P_\mathrm{r}}}{2}Y^*(f)H\left(f-f_\mathrm{c};\mathrm{TEC}\right) + \frac{\sqrt{P_\mathrm{r}}}{2}Y(f)H\left(f+f_\mathrm{c};\mathrm{TEC}\right) \tag{17}$$

and

$$\mathcal{F}\{s_\mathrm{Q}(t;\boldsymbol{\theta})\} = \frac{j\sqrt{P_\mathrm{r}}}{2}Y^*(f)H\left(f-f_\mathrm{c};\mathrm{TEC}\right) - \frac{j\sqrt{P_\mathrm{r}}}{2}Y(f)H\left(f+f_\mathrm{c};\mathrm{TEC}\right) \tag{18}$$

where

$$\boldsymbol{\theta} = \left[\mathrm{TEC}, P_\mathrm{r}\right]^\mathrm{T} \tag{19}$$

Finally, the complex envelope of the received signal can be given by:

$$\begin{aligned}\mathcal{F}\{s(t;\boldsymbol{\theta})\} &= \mathcal{F}\{s_\mathrm{I}(t;\boldsymbol{\theta}) + js_\mathrm{Q}(t;\boldsymbol{\theta})\} = \sqrt{P_\mathrm{r}}Y(f)H\left(f-f_\mathrm{c};\mathrm{TEC}\right) \\ &= \sqrt{P_\mathrm{r}}(Y_\mathrm{I}(f) + jY_\mathrm{Q}(f))H\left(f-f_c;\mathrm{TEC}\right)\end{aligned} \tag{20}$$

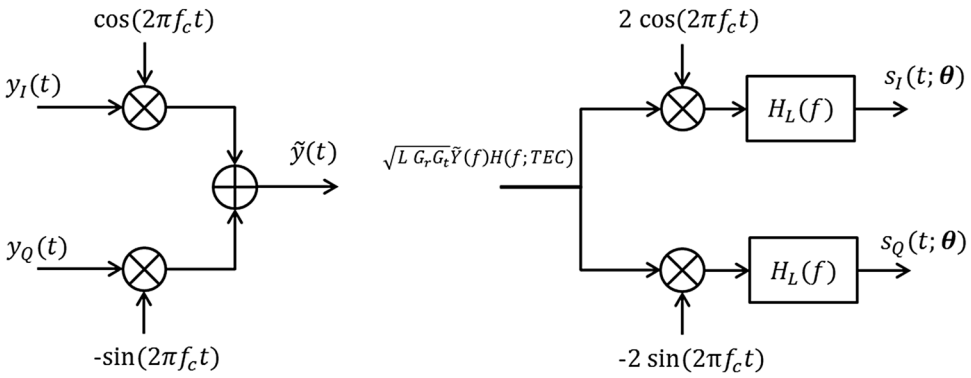

Fig. 1 Transmit bandpass signal after signal generation on the satellite, propagation, and baseband receive signal model after down conversion and low-pass filtering

In the next section, after discussing ionospheric propagation and defining the signal model we derive an estimator for TEC and the receive power P_r of the signal.

Maximum likelihood estimation of TEC and received power based on binned data

We consider N observations of a random vector $\boldsymbol{x}$ which has a multivariate Gaussian probability density function (pdf) parameterized by the parameter vector $\boldsymbol{\theta}$, denoted by $p_{\boldsymbol{x}}(\boldsymbol{x}[n];\boldsymbol{\theta})$. The realization of the random variable $\boldsymbol{x}$ at time instant n is given by $\boldsymbol{x}[n]$ and $n = 1, \ldots, N$. The pdf is given by:

$$p_{\boldsymbol{x}}(\boldsymbol{x}[n];\boldsymbol{\theta}) = \frac{1}{\sqrt{2\pi\sigma_n^2}} \exp\left[-\frac{\boldsymbol{x}[n] - \boldsymbol{s}[n;\boldsymbol{\theta}]_2^2}{2\sigma_n^2}\right] \tag{21}$$

where the discrete signal model with $t = nT_s$ and $T_s = 1/2B$ can be given by

$$\boldsymbol{x}[n] = \begin{bmatrix} x_I[n] \\ x_Q[n] \end{bmatrix} = \boldsymbol{s}[n;\boldsymbol{\theta}] + \boldsymbol{n}[n] = \begin{bmatrix} s_I[n;\boldsymbol{\theta}] \\ s_Q[n;\boldsymbol{\theta}] \end{bmatrix} + \begin{bmatrix} n_I[n] \\ n_Q[n] \end{bmatrix} \in \mathbb{R}^{2\times 1} \tag{22}$$

Here, $x_I[n]$ and $x_Q[n]$ are the inphase and quadrature components of the received signal and $n_I[n]$ and $n_Q[n]$ are the inphase and quadrature components of the additive noise with variance σ_n^2. We assume that the noise is white Gaussian and proper. The likelihood is given by:

$$L(\boldsymbol{x}[n];\boldsymbol{\theta}) = p_{\boldsymbol{x}}(\boldsymbol{x}[n];\boldsymbol{\theta}) \tag{23}$$

For large data samples ($N \to \infty$) the log-likelihood function becomes difficult to compute since one has to sum $\log(L(\boldsymbol{x}[n];\boldsymbol{\theta}))$ for all observations N. In such cases instead of recording all the observations we can build a histogram with a number of entries $\boldsymbol{b} = \left[b_1, \ldots, b_M\right]^T \in \mathbb{N}_0^{M\times 1}$ in M bins with $m = 1, \ldots, M$ as outlined in Cowan (1998). The expectation $\epsilon(\boldsymbol{\theta}) = \left[\epsilon_1(\boldsymbol{\theta}), \ldots, \epsilon_M(\boldsymbol{\theta})\right]^T \in \mathbb{N}_0^{M\times 1}$ of the number of entries b_m can be given by:

$$\epsilon_m(\boldsymbol{\theta}) = \sum_{\boldsymbol{x}_m^{\min} \le \boldsymbol{x}[n] < \boldsymbol{x}_m^{\max}} L(\boldsymbol{x}[n];\boldsymbol{\theta}) = N\, p_m(\boldsymbol{\theta}) \tag{24}$$

where $\boldsymbol{x}_m^{\min}$ and $\boldsymbol{x}_m^{\max}$ are the bin limits of the histogram and $p_m(\boldsymbol{\theta})$ is the probability of an entry in the m-th bin of the histogram. We define vector inequality, as used above in (24), of two vectors $\boldsymbol{o} = \left[o_1, \ldots, o_N\right]^T$ and $\boldsymbol{p} = \left[p_1, \ldots, p_N\right]^T$ with $\boldsymbol{o}, \boldsymbol{p} \in \mathbb{R}^{N\times 1}$ as:

$$\boldsymbol{o} \le \boldsymbol{p} \quad \text{if } \forall_{i=1}^N o_i \le p_i \tag{25}$$

$$\boldsymbol{o} < \boldsymbol{p} \quad \text{if } \forall_{i=1}^N o_i < p_i \tag{26}$$

$$\boldsymbol{o} \ge \boldsymbol{p} \quad \text{if } \forall_{i=1}^N o_i \ge p_i \tag{27}$$

$$\boldsymbol{o} > \boldsymbol{p} \quad \text{if } \forall_{i=1}^N o_i > p_i \tag{28}$$

One can regard the histogram as a single measurement of an M-dimensional random vector $\boldsymbol{b}$ with a realization $\boldsymbol{b}$ for which the joint pdf is given by a multinomial distribution, as shown in Cowan (1998),

$$p_{\boldsymbol{b}}(\boldsymbol{b};\epsilon(\boldsymbol{\theta})) = \frac{N!}{b_1! \ldots b_M!} \left(\frac{\epsilon_1(\boldsymbol{\theta})}{N}\right)^{b_1} \cdots \left(\frac{\epsilon_M(\boldsymbol{\theta})}{N}\right)^{b_M} \tag{29}$$

Thus, the probability to be in bin m is expressed as the expectation $\epsilon_m(\boldsymbol{\theta})$ divided by the number of observations N. The log-likelihood is given by:

$$l(\boldsymbol{\theta}) = \log\left(L(\boldsymbol{b};\epsilon(\boldsymbol{\theta}))\right) = \log\left(p_{\boldsymbol{b}}(\boldsymbol{b};\epsilon(\boldsymbol{\theta}))\right) \tag{30}$$

Dropping all terms that are not dependent on θ we can write

$$l(\boldsymbol{\theta}) = \arg\max_{\boldsymbol{\theta}} \sum_{m=1}^{M} b_m \log\left(\epsilon_m(\boldsymbol{\theta})\right) \tag{31}$$

In our case, this mathematical expression can be solved by a grid-search in $\boldsymbol{\theta}$ based on (14) using an appropriate model for $s_I(t;\boldsymbol{\theta})$ and $s_Q(t;\boldsymbol{\theta})$ following (17) and (18) to derive $\epsilon_m(\boldsymbol{\theta}) = N\, p_m(\boldsymbol{\theta})$. On the other hand, based on the histogram derived from the measurement data $\boldsymbol{x}[n]$ using the same bin limits $\boldsymbol{x}_m^{\min}$ and $\boldsymbol{x}_m^{\max}$ we can derive the number of entries for each bin b_m.

Additionally, the receive antenna gain of the used high-gain antenna is $G_r \approx 50$ dB and the beamwidth of the antenna is so small that the signal of only one GNSS satellite is received with a signal-to-noise-ratio (SNR) of approximately 25–30 dB. Thus, the histogram of $\boldsymbol{x}[n]$ with bin limits $\boldsymbol{x}_m^{\min}$ and $\boldsymbol{x}_m^{\max}$ resembles the so-called signal modulation constellation diagram. Usually, the signal modulation constellation diagram is depicted in a two-dimensional graph with $x_I[n]$ on the horizontal axis and $x_Q[n]$ on the vertical axis and a color scale showing the absolute frequency of entries in the bins.

In the next section, we discuss the influence of ionospheric dispersion on broadband GNSS signals. Furthermore, we will show how to generate the expectation of the number of entries $\epsilon(\boldsymbol{\theta})$ in order to perform sTEC estimates and corrections using the maximum likelihood estimator based on binned data as given in (31). Afterwards, we will assess the performance of the proposed estimator given in (31) using the high gain antenna measurement data.

Ionospheric dispersion affecting broadband signals

Following the approach of Gao et al. (2007), we will now apply the ionospheric dispersion to simulate complex signals in the frequency domain and investigate its impact on

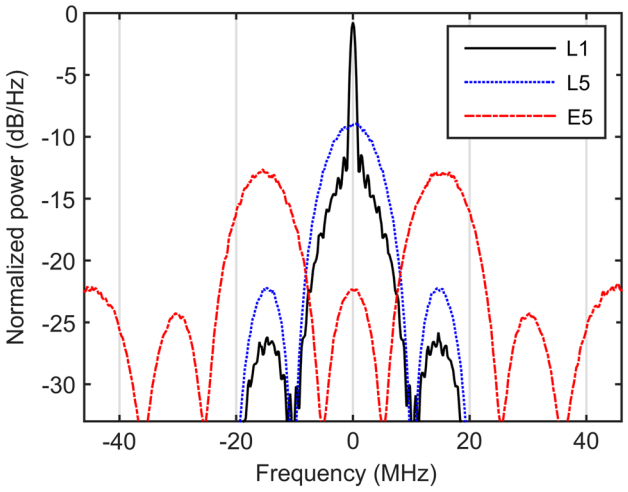

Fig. 2 Power spectral density of the simulated L1, L5, and E5 signals

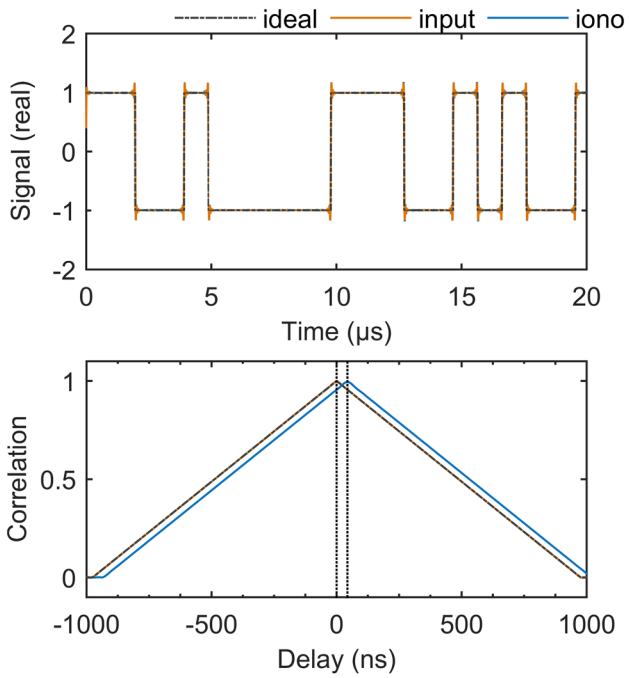

Fig. 3 Simulated ionospheric effect of 80 TECU on the GPS L1 signal. The top plot shows the real part (C/A) of the signal before and after traversing the ionosphere and the bottom plot the corresponding correlation functions with an ideal signal. For better illustration, the constant time delay at the carrier frequency has been removed in the top plot. The dashed lines in the bottom plot mark the calculated group delay at the carrier frequency

the signal shape in the time domain. In particular, we will compare its influence on three different GNSS signals, GPS L1, GPS L5 and Galileo E5, with a bandwidth ranging from 2 MHz to about 50 MHz in their main lobes as depicted in Fig. 2. For the broadband signals, a significant focus is set on the deformation of the signal modulation constellation diagram, as defined in the previous section, which is not usually accessible to the user, but detectable by high gain antenna measurements with sufficient antenna gain.

For GPS L1 the simulation result at 80 TECU is shown in Fig. 3. Note that for simplicity only the real part of the signal is shown in the figure even though a complex signal with P-code in the quadrature component was used in the calculation. This is important since the orthogonality of the C/A and the P-code signals is partially lost because of the dispersive nature of the ionosphere.

Nevertheless, the overall effect is small in the case of the narrow band L1 signal. The C/A chips depicted in the top panel of Fig. 3 deviate from the ideal signal (gray line) mainly because of the additional band limitation and a difference between the clean (orange) and ionosphere affected (blue) signal is barely visible. In consequence, the correlation function is merely shifted by the delay calculated for the carrier frequency but otherwise virtually unaffected by the ionosphere (see bottom panel of Fig. 3). It is important to note that the correlation functions shown throughout this article represent the absolute value of the cross-correlation between the respective complex signal and the real part of its ideal code replica. Hence, the observed power loss in the correlation peak is minimal in this representation.

Turning to the GPS L5 signal (Fig. 4), we keep the QPSK modulation but increase the bandwidth by one order of magnitude. At the same time, the absolute delay is more significant, and the dispersion is more severe at the L5 carrier frequency compared to L1. Still, the ionospheric impact on the chip shape (blue line in top panel of Fig. 4) is small. The slightly visible distortion compared to the unperturbed signal (orange) mainly results from cross-talk between in-phase and quadrature component caused by the dispersive phase shift. The ripples visible in both signals are a result of the further band limitation according to the GPS specifications. Noteworthy, this limitation already causes a deformation of the correlation function with the ideal signal as illustrated in the middle panel of Fig. 4. Apart from the constant delay, the ionospheric effect on the correlation function appears to be negligible.

Influence of the ionosphere is clearly visible in the signal modulation constellation histogram. Ideally, the L5 constellation would consist of four distinct points marking the corners of a square. Band limitation and sampling of the unperturbed signal result in elongated constellation features pointing in the direction of the diagonals of the square (left bottom panel of Fig. 4). These features are slightly tilted counterclockwise, away from the diagonals by the ionosphere (right bottom panel of Fig. 4) an effect that scales with the total electron content.

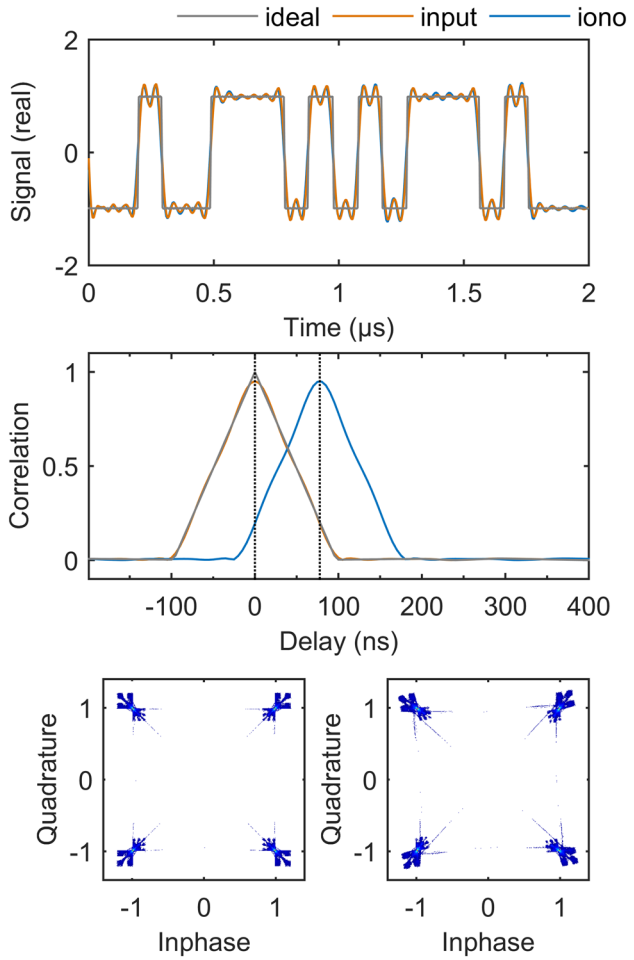

Fig. 4 Simulated ionospheric effect of 80 TECU on the GPS L5 signal. The top plot shows the real part of the signal before and after traversing the ionosphere and the middle plot the corresponding correlation functions. The signal modulation constellation histograms without and with ionospheric effect are shown in the bottom two plots, respectively. For better illustration, the constant time delay at the carrier frequency has been removed in the top plot. The dashed lines in the middle plot mark the calculated group delay at the carrier frequency

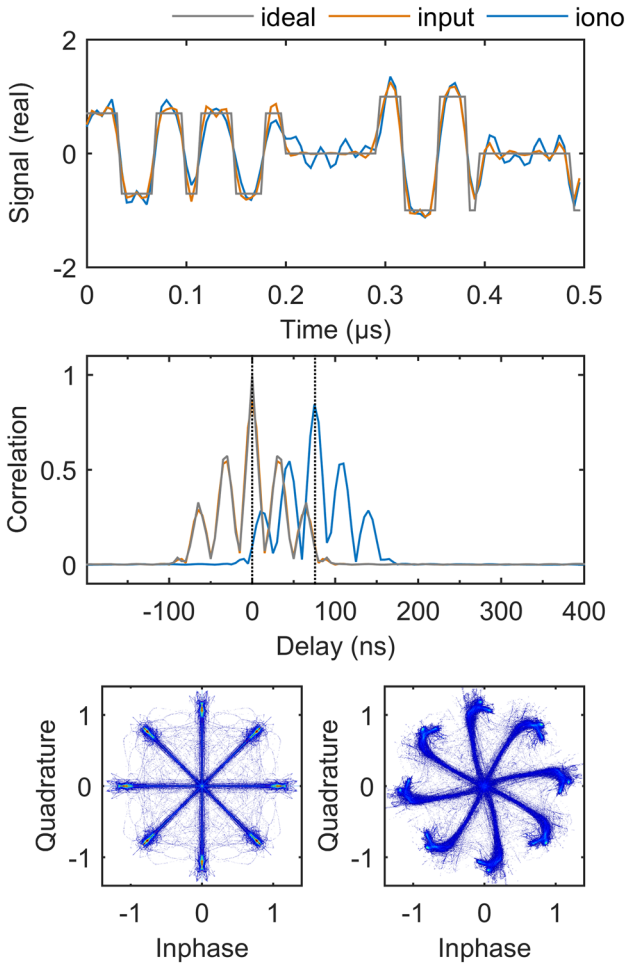

Fig. 5 Simulated ionospheric effect 80 TECU on the Galileo E5 signal. The top plot shows the real part of the signal before and after traversing the ionosphere and the middle plot the corresponding correlation functions. The signal modulation constellation histograms without and with ionospheric effect are shown in bottom two plots, respectively. For better illustration, the constant time delay at the carrier frequency has been removed in the upper plot. The dashed lines in the middle plot mark the calculated group delay at the carrier frequency

Finally, we investigate the Galileo E5 signal (Fig. 5). The bandwidth of its main lobes spans about 50 MHz, and the major fraction of the signal power is far from the center frequency due to the AltBOC modulation (see Fig. 2).

The signal is broadcast at a carrier frequency close to GPS L5 and is band-limited to about 92 MHz, resulting in an unperturbed signal represented by the orange curve in the top panel of Fig. 5. Applying a simulated ionosphere of 80 TECU leads to a signal distortion which is now clearly visible in the chip shape (blue). The overall influence on the correlation function remains small: its symmetry is preserved, and the power loss at the peak maximum is less than 2% compared to the clean signal.

Severe changes, however, are seen in the signal modulation constellation histogram: band limitation and sampling transform the ideal constellation, eight points equally spaced on the unit circle, into elongated features connected by the chip transitions in a star-shaped manner (left bottom panel of Fig. 5). The dispersion of the ionosphere rotates the constellation points and smears out the features resulting in a "spiral-shaped" constellation diagram (right bottom panel of Fig. 5). Clearly, for Galileo E5, the constellation diagram is highly susceptible to the ionospheric conditions, and the deformation becomes more pronounced with increasing electron content as illustrated in Fig. 6.

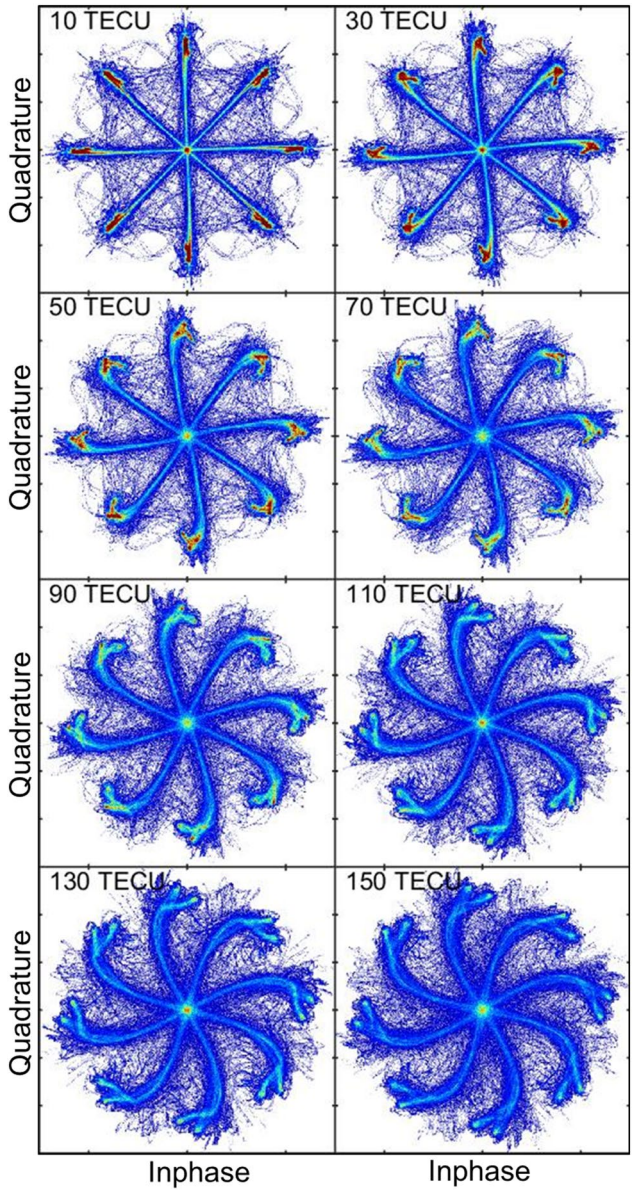

Fig. 6 Simulation of the influence of different electron content on the Galileo E5 signal modulation constellation diagram (histogram). All graphs share a common color bar. Red indicates a high, blue a low number of bin entries

Estimation of sTEC and broadband ionospheric correction

From the simulation results of the previous section, two real-world applications come to mind: first, instead of merely accounting for a constant delay caused by a given TEC, a receiver can also correct the ionospheric distortion (dispersion) easily by multiplying the complex conjugate of the phase shift in (13) to the signal. Second, we propose that the characteristic distortion of the signal modulation constellation diagram is exploited to estimate the ionospheric

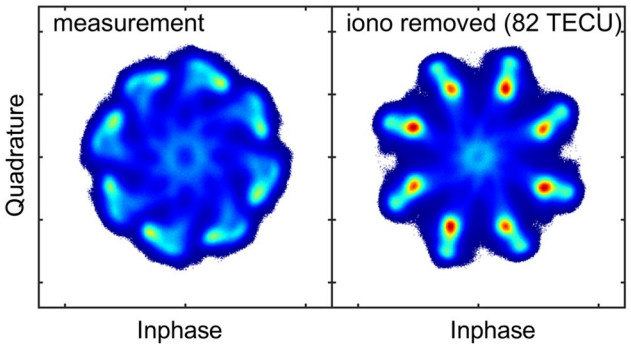

Fig. 7 Constellation histogram of Doppler corrected Galileo E5 measurement data without (left) and with an ionospheric correction of estimated 82 TECU applied (right)

TEC as described in (21)–(31), especially in the case of high gain antenna measurements (Thoelert et al. 2013). Figure 7 illustrates the working principle of the maximum likelihood TEC estimator as described in (31).

The left panel of Fig. 7 shows the constellation histogram of a measured and Doppler corrected Galileo E5 signal. Clearly, its "buzz saw blade" shape resembles what was observed in the simulation presented in the right bottom panel of Fig. 5. Moreover, indeed, if the measured signal is corrected with the dispersive ionospheric model at 82 TECU the signal power is shifted remarkably close to the nominal constellations shown in the right part. We attribute the remaining distortion to the satellite payload, the antenna phase, and noise. Nevertheless, the striking improvement of the signal shape is a reliable indicator that the TEC was correctly estimated.

We have also analyzed a complete satellite path with data acquisitions every 5 min and performed sTEC estimations using each snapshot. Figure 8 shows the result of the TEC estimation based on the Doppler corrected I–Q-samples and based on the method described in this research. In comparison, the TEC values calculated based on a vTEC map, are presented. For this processing, the simple thin-shell ionospheric layer model has been used to convert the vTEC map information into sTEC values corresponding to the signal propagation path.

Furthermore, a GNSS receiver (Septentrio PolaRx4TR) was connected in parallel to the high-gain antenna during the I–Q-sample recording. Dual-frequency GNSS observables can be used to calculate the sTEC values. The challenge in this approach is the correction of the additional biases based on the satellite payload and GNSS receiver behavior. The first one can be compensated using IGS MGEX products. Using the provided differential code bias (DCB) of the observed satellite, a TEC map, and measurement observables, one can calculate the DCB of the used receiver. For this procedure, the discrepancy

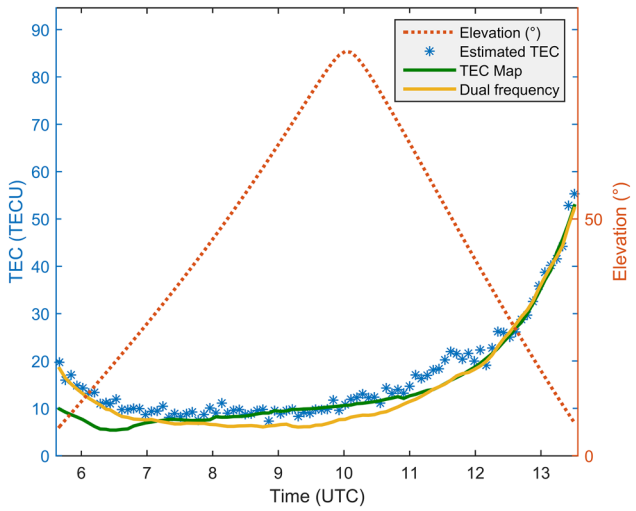

Fig. 8 Slant TEC values are shown regarding a satellite path observed from Weilheim ground station, Germany on November 26, 2015. The blue stars represent the TEC estimates based on the IQ data. The dark green curve represents slant TEC values calculated by a vTEC map and the use of the thin-shell ionospheric layer model. The yellow curve shows TEC estimates based on receiver measurements recorded at the same station. The dashed red curve represents the elevation of the space vehicle according to the receiving station

Table 1 Mean and standard deviation of ionospheric TEC estimation based on the I–Q-samples related to the TEC map and GNSS receiver results, respectively

Ionospheric TEC estimates based on I–Q-samples compared to:	Mean difference (TECU)	Standard deviation (TECU)
Dual frequency	2.4	1.6
TEC map	2.1	2.5

between the TEC map information and the actual ionospheric conditions during the calibration has to be negligible. To achieve this, receiver observables at high elevation during a night-time satellite pass were utilized, when the vertical and slant TEC are nearly identical, and the absolute influence of the ionosphere is minimal. Now one can determine the sTEC based on the GNSS dual-frequency measurements. These results are also shown in Fig. 8.

The mean and standard deviation of the relation of ionospheric TEC estimation based on the I–Q-samples regarding the TEC map and the GNSS receiver results are given in Table 1, respectively. The histogram of the residuals between the results of the I–Q-samples based method and the TEC map as well as the GNSS receiver results are shown in Fig. 9.

The residuals show good performance of our proposed method in comparison to the other two common ionospheric TEC estimation methods, using TEC maps or a GNSS receiver connected to the high gain antenna. A literature review provides an accuracy between 2 and 9 TECU according to IGS TEC map products (Johnston et al. 2017) and around 1 TECU (RMS) for very precise TEC map products (Jakowski 2017). However, also note that TEC map products can differ up to 12 TECU (Li et al. 2017). For low TEC (low TECU), we can observe that the results of the proposed method are by trend a bit higher compared to the results of the other two methods. For higher TEC (high TECU), the results seem to be slightly more stable (see Fig. 8 for TEC higher than 20 TECU). The residual distribution within the histograms shows a non-Gaussian behavior.

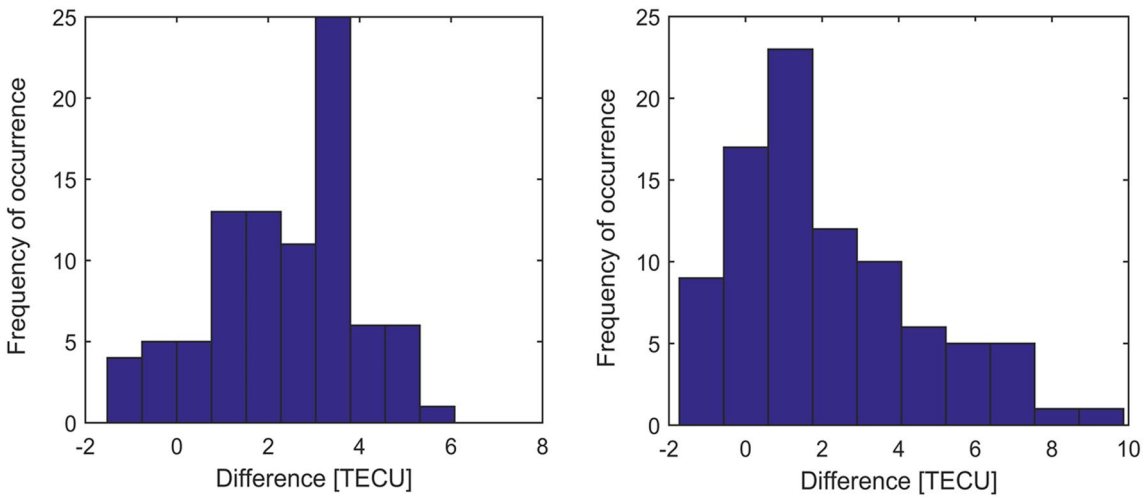

Fig. 9 Histogram of the residuals between IQ estimation results and GNSS receiver TEC estimation (left) and TEC map (right)

Conclusion

Starting from a recapitulation of ionospheric dispersion of radio signals, we have investigated its impact on three different GNSS signals of different bandwidth and modulation. While confirming previous reports (Gao et al. 2007; Henkel et al. 2009), we have put a significant emphasis on the deformation of the signal modulation constellation diagram, which is not normally accessible for receivers. With a particular focus on high gain antenna measurements, we have proposed a new method to estimate the ionospheric electron content directly from the single frequency signal. We have demonstrated that the proposed method to estimate slant TEC based on I–Q-samples from a high-gain antenna performs at least as well as methods based on TEC maps or using a calibrated GNSS receiver connected to the high gain antenna (dual-frequency measurements). We would like to point out that high-gain antenna measurements are independent of code correlation. Additionally, the received signal is de facto unaffected by multipath and interference because of the narrow aperture angle (0.5°) of the antenna. Our proposed method thus is inherently free of these uncertainties that might otherwise be critical in the case of conventional GNSS receiver measurements.

Acknowledgements The authors want to thank the colleagues from the German Space Operation Center (GSOC), at the DLR ground station Weilheim for supporting and operating the high-gain antenna. Furthermore, the authors thank our colleagues Volker Wilken, Martin Kriegel, Jens Berdermann and Mainul Hoque from DLR Neustrelitz, for the provision of high-resolution TEC maps.

References

Cowan G (1998) Statistical data analysis. Clarendon Press, Oxford

European GNSS (Galileo) Open Service (2015) Ionospheric correction algorithm for Galileo single frequency users. Technical report

Gao GX, Datta-Barua S, Walter T, Enge P (2007) Ionosphere effects for wideband GNSS signals. In: Proceedings of ION ATM, Institute of Navigation, April 23–25, Cambridge, MA, USA, pp 147–155

Garbuny M (1965) Optical physics. Acadamic Press, New York

Henkel P, Gao GX, Walter T, Günther C (2009) Robust multi-carrier, multi-satellite vector phase locked loop with wideband ionospheric correction and integrated weighted RAIM. In: Proceedings of ENC GNSS 2009, Naples, Italy

Hernandéz-Pajares M, Juan JM, Sanz J (1999) New approaches in global ionospheric determination using ground GPS data. J Atmos Sol Terr Phys 61(16):1237–1247

Hobinger T, Jakowski N (2017) Atmospheric signal propagation. In: Teunissen PJ, Montenbruck O (eds) Springer handbook of global navigation satellite systems. Springer, Berlin, pp 165–194

Hoque MM, Jakowski N (2008) Mitigation of higher order ionospheric effects on GNSS users in Europe. GPS Solut 12(2):87–97. https://doi.org/10.1007/s10291-007-0069-5 **(ISSN 1521–1886)**

Jakowski N (1996) TEC monitoring by using satellite positioning systems. In: Kohl H, Ruester R, Schlegel K (eds) Modern ionospheric science. European Geophysical Society, Munich, pp 371–390

Jakowski N (2017) Ionosphere monitoring. In: Teunissen PJ, Montenbruck O (eds) Springer handbook of global navigation satellite systems. Springer, Berlin, p. 1143 **(Fig. 39.5)**

Jakowski N, Mayer C, Hoque MM, Wilken V (2011) Total electron content models and their use in ionosphere monitoring. Radio Sci 46(6):RS0D18

Johnston G, Riddell A, Hausler G (2017) The international GNSS service. In: Teunissen PJ, Montenbruck O (eds) Springer handbook of global navigation satellite systems. Springer, Berlin, pp 967–981

Kelley MC (2009) Earth's ionosphere: plasma physics and electrodynamics. Elsevier, Burlington

Klobuchar JA (1987) Ionospheric time-delay algorithm for single-frequency GPS users. IEEE Trans Aerosp Electron Syst 23(3):325–331. https://doi.org/10.1109/TAES.1987.310829

Li M, Yuan Y, Wang N, Li Z, Li Y, Huo X (2017) Estimation and analysis of Galileo differential code biases. J Geodesy 91(3):279–293. https://doi.org/10.1007/s00190-016-0962-1

Marques HA, Monico JFG, Rosa GPS, Chuerubim ML, Aquino M (2012) Second and third order ionospheric effects on GNSS positioning: a case study in Brazil. Geodesy Planet Earth IAG Symp 136:619–625

Sardón E, Rius A, Zarraoa N (1994) Estimation of the transmitter and receiver differential biases and the ionospheric total electron content from Global Positioning System observations. Radio Sci 29(3):577–586. https://doi.org/10.1029/94RS00449

Thoelert S, Furthner J, Meurer M (2013) GNSS survey—signal quality assessment of the latest GNSS satellites. In: Proceedings of ION ITM 2013, Institute of Navigation, January 28–30, San Diego, USA, pp 608–615

Ya'acob N, Abdullah M, Ismail M (2008) Determination of GPS total electron content using single layer model (SLM) ionospheric mapping function. Int J Comput Sci Netw Secur 8(9):154–160

Zolesi B, Cander LR (2014) Ionospheric prediction and forecasting. Springer, Berlin, ISBN 978-3-642-38430-1

Ulrich Hörmann studied physics in Augsburg (Germany) and Karlstad (Sweden). He received his Ph.D. in physics from the University of Augsburg in 2015 and joined the Institute of Communications and Navigation at the German Aerospace Center (DLR) with his focus on GNSS signal monitoring. Recently, he has moved to the Institute of Physics and Astronomy at the University of Potsdam.

Steffen Thoelert received his diploma degree in electrical engineering from the University of Magdeburg in 2002. In May 2006 he joined the Institute of Communications and Navigation at the German Aerospace Centre (DLR), Oberpfaffenhofen. His current research activities include signal quality monitoring, satellite payload characterization, system calibration, GNSS compatibility and interference aspects.

Matteo Sgammini received the M.Eng. degree in electrical engineering in 2005 from the University of Perugia. He joined the Institute of Communications and Navigation of DLR in 2008. He is currently pursuing a Ph.D. in electrical engineering with research interests in interference mitigation techniques for GNSS. Current research activity includes adaptive filtering, array signal processing and estimation theory for GNSS.

Christoph Enneking received the BSc. and the MSc. degrees in electrical engineering from the Munich University of Technology (TUM), Germany, in 2012 and 2014, respectively. In September 2014, he joined the Institute of Communications and Navigation of the German Aerospace Center (DLR), Wessling-Oberpfaffenhofen. His research interests include GNSS signal design, estimation theory, and GNSS intra- and intersystem interference.

Johann Furthner received his Ph.D. in Physics in the field of laser physics at the University of Regensburg (Germany) in 1994. Since 1995 he is scientific staff at German Aerospace Centre (DLR). In 2008 he stayed a half year at ESA in the Galileo Project Team. He is working on the development of navigation systems in a number of areas.

Michael Meurer received the diploma in Electrical Engineering and the Ph.D. degree from the University of Kaiserslautern, Germany. Since 2006 he is the director of the Department of Navigation of the German Aerospace Center (DLR). In addition, he is a professor of electrical engineering and director of the Chair of Navigation at the RWTH Aachen University. His current research interests include GNSS signals, GNSS receivers, and navigation for safety-critical applications.

Felix Antreich received the Diploma degree in electrical engineering from the Munich University of Technology (TUM), Munich, Germany, in 2003. In 2011 he also received the Doktor-Ingenieur (Ph.D.) degree from the TUM. Since September 2016 he is a visiting professor in the Department of Teleinformatics Engineering (DETI) at the Federal University of Ceará (UFC) in Fortaleza, Brazil.